Desalination and Water Treatment
www.deswater.com

doi: 10.5004/dwt.2019.23597

146 (2019) 373–384
April

Preparation of magnetic mesoporous carbon based on polydopamine and their superperformance for adsorption of dye pollutants

Xiguang Liu[a], Shengxiao Zhang[a,*], Zongyuan Zhang[a], Xingxing Liu[a], Qiaoli Zhang[a], Yuanyuan Zhang[b], Qiang Xu[a], Hui Xu[a], Juan Jin[a], Yubao Wang[a,*]

[a]*Collaborative Innovation Center of Shandong Province for High Performance Fibers and Their Composites, School of Chemistry and Materials Science, Ludong University, Yantai 264025, Shandong province, China, Tel. +86 535 6672176; Fax +86 535 695905; emails: beijingzsx@163.com (S. Zhang), wangyubao1969@163.com (Y. Wang), xgliu1986@163.com (X. Liu), 876884139@qq.com (Z. Zhang), 1446847673@qq.com (X. Liu), 799682145@qq.com (Q. Zhang), lduxuqiang@126.com (Q. Xu), xuhui235@163.com (H. Xu), jinjuan8341@163.com (J. Jin)*
[b]*Yantai Environmental Monitoring Center, Yantai 264025, Shandong province, China, email: jinanzyy@163.com*

Received 11 June 2018; Accepted 13 December 2018

ABSTRACT

Dopamine self-polymerized on the pore channel of SBA-15 as carbon precursor, and Fe^{3+} coordinated with polydopamine (PDA) as iron source to prepare a novel material. After calcination at 600°C for 2 h, PDA was carbonized and Fe^{3+} was converted to magnetic nanoparticles. Then the SBA-15 template was dissolved with 3 mol/L ethanol–NaOH solution, magnetic mesoporous carbon (MMC) material was obtained. The resulted MMC was characterized by various instruments, and the results proved that tiny magnetic nanoparticles were distributed uniformly on the carbon matrix, and mesoporous structure of the carbon substrate was confirmed. Three organic dyes were selected as target pollutants to investigate the adsorption behavior of MMC. Under the optimal condition, the maximum adsorption capacity calculated from Langmuir adsorption isotherm for congo red, neutral red and methyl green were 2,315.4; 2,431.6 and 2,927.1 $mg \cdot g^{-1}$, respectively. Furthermore, the maximum adsorption capacity in natural water showed no obvious decrease, indicating strong anti-interference ability of the sorbents. Gibbs free energy calculated from thermodynamics data was negative, demonstrating that the adsorption was a spontaneous process. Due to the excellent adsorption performance of carbon material, high specific surface area, and a large number of adsorption sites on the mesoporous structure, the MMC showed ultrahigh adsorption capacity for organic dyes, indicating its great potential for dye pollutants removal.

Keywords: Dopamine; Magnetic nanoparticle; Mesoporous carbon; Adsorption; Dye

1. Introduction

Mesoporous materials form a category of porous materials with pore diameter between 2 and 50 nm [1,2], which have some remarkable properties, such as ultrahigh surface areas, large pore volumes, tunable pore sizes and shapes, and also exhibit nanoscale effects in their mesochannels and on their pore walls [3]. Ordered mesoporous carbons have attracted wide interest in the field of adsorption [4–7], catalysis [8,9] and energy storage [10–12]. The general pathways for the synthesis of mesoporous carbons include soft-templating [13–16] and hard-templating [17–19] methods. Zhao et al. [20] prepared large-pore ordered mesoporous silica SBA-15 with a 2D hexagonal structure by using triblock copolymers as templates, which was usually chosen as a hard template due to its regular pore structure, high surface area, and reliable and easy synthesis method, and the unique hexagonal array

* Corresponding authors.

of pore structures of SBA-15 was beneficial to form a nice carbon skeleton under the silica template. It is also important to choose a proper carbon source for mesoporous carbon. Carbon precursor is always expected to have high carbon yield and proper molecular size to match the template agent channel. A numerous carbon sources are reported including saccharides [21–24], resins [15,16], arene [25] and so on.

Though mesoporous carbon owns excellent property, the difficulty of separation from solution limits its application. In recent years, application of magnetic nanomaterials for removal of various pollutants was widely explored [26–31]. Magnetic nanoparticle can be separated from solution with a magnet easily and redispersed rapidly as soon as the magnet is taken away due to its superparamagnetism, which facilitates collection, regeneration and recycling of the materials. If magnetic nanoparticle is introduced into the mesoporous carbon material, magnetic mesoporous carbon (MMC) with high saturation magnetic intensity will be obtained, which not only remains the advantage of the mesoporous carbon, but also benefits for the separation and regeneration of the composites. There were some reports about the preparation and application of MMCs with core-shell [32–34] and decorated [35–37] structure. Nevertheless, the application of these materials might be always limited by the time-consuming tedious operation or the disturbance to ordered mesoporous structure with the introduction of magnetic nanoparticle.

Dopamine, as a biomimetic small molecule compound, shows excellent feature of spontaneous polymerization under seawater condition just similar to adhesive proteins secreted by mussel, and it can self-assemble to form a coating layer on the surface of various substrates [38,39]. Dopamine is an excellent carbon source because it has a structure similar with phenolic resin with high carbon yield as well [40]. Furthermore, polyphenol compounds can coordinate with Fe^{3+} to form a cross-linked polymer [41]. Zhou et al. [42] proved that Fe^{3+}-dopamine complexation could be converted into carbon shell and well-dispersed tiny Fe_3O_4 nanoparticles by annealing at 750°C. If dopamine and Fe^{3+} can auto-polymerize on the pore channel of SBA-15, and then polydopamine is carbonized and Fe^{3+} converts to magnetic nanoparticles under high-temperature calcination, it will obtain MMC material after the SBA-15 template is dissolved. The proposed preparation process of MMC based on polydopamine and Fe^{3+} with SBA-15 as hard template is shown in Fig. 1.

With the mass production and use of the organic dyes in industry, dye wastewater treatment has become a crucial challenge for its deep chromaticity and great toxicity, which results in great influence on environment and our lives. Thus, it is urgent to develop effective methods to solve this environmental problem. Adsorption method provides a simple, economic and effective way to remove various organic pollutants [43,44]. MMC, which owns high surface area, large pore volume, strong adsorptivity, and magnetic separation, has great potential for removal of organic dye pollutants.

Herein, in this study, MMC was prepared using SBA-15 as a hard template, Fe^{3+} as iron source, and polydopamine (PDA) as carbon precursor, respectively. Three organic dyes were selected as targeted pollutants to study the adsorption performance of the resulted MMC, and the effect of solution pH, ionic strength, adsorption isotherms, kinetics, and thermodynamics were all investigated in detail.

2. Experimental section

2.1. Materials and reagents

Dopamine, pluronic P-123 (EO20-PO70-EO20, M_a = 5,800), and tetraethyl orthosilicate (TEOS) were obtained from Sigma-Aldrich Corp. (Germany). Anhydrous, ferric chloride ($FeCl_3$), and tris (3-hydroxymethyl aminomethane) were supplied from Sinopharm Chemical Reagent Co., Ltd. (Beijing, China). Congo red, neutral red and methyl green were purchased from Damao Chemical Reagent Corporation

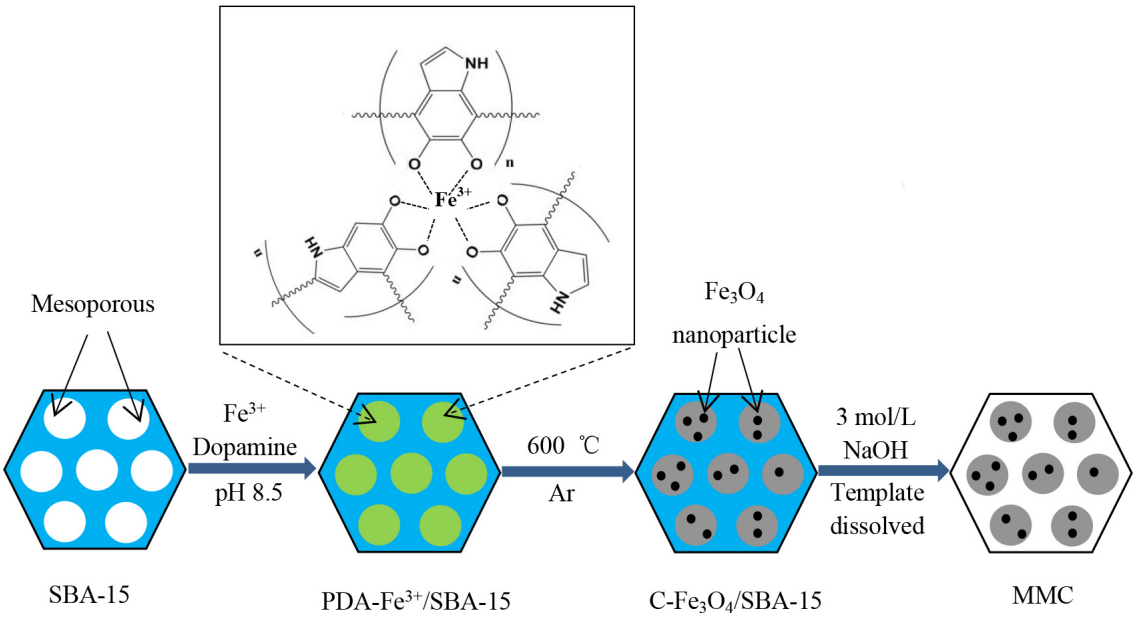

Fig. 1. Schematic diagram of preparation of MMC based on polydopamine and Fe^{3+} with SBA-15 as hard template.

(Tianjin, China). Pure water used in experiment was obtained from a Millipore purification system (Bedford, MA, USA).

2.2. Synthesis of mesoporous silica (SBA-15) and magnetic mesoporous carbon

The SBA-15 was prepared using the method described in the literature [20]. In a typical procedure, P123 (1.0 g) were added in the 30 mL HCl solution (2 mol L^{-1}), and the mixture was stirred at 36°C until it turned into a homogeneous solution. Then 2.08 g TEOS were added and the solution was stirred continuously for 24 h. Subsequently, the solution was transferred into a polytetrafluoroethylene-lined autoclave, and maintained at 100°C for 24 h. After it cooled to room temperature, the product was collected by filtration and washed with pure water for several times, and then dried at room temperature. The resulted powder was calcined at 550°C for 5 h under air atmosphere in a tube furnace, and then naturally cooled to room temperature to obtain the SBA-15 material.

MMC was prepared by using mesoporous silica SBA-15 as a hard template, $FeCl_3$ as iron source, and PDA as carbon precursor, respectively. Briefly, 0.5 g SBA-15 was dispersed in 75 mL solution containing 1.5 g dopamine and 0.5 g $FeCl_3$, and 0.2 g tris was added to adjust solution pH to about 8.5. The mixture was stirred at 25°C for 24 h, and then the suspended solid was collected by filtration and washed with pure water. After dried at 35°C, black powder was obtained. The powder was calcined at 600°C for 2 h under argon atmosphere at a heating rate of 1°C/min in a tube furnace, and then naturally cooled to room temperature.

To remove the SBA-15 template, the carbon–silica composite was immersed in 3 mol/L ethanol–NaOH solution (50 vol% H_2O and 50 vol% ethanol) for 5 h at 80°C under reflux. After naturally cooled to room temperature, the MMC was separated with a magnet and washed with pure water, and finally dried at 35°C for 24 h. For comparison, mesoporous carbon (MC) was prepared according to the abovementioned process except for no $FeCl_3$ addition.

2.3. Characterization

The particle size and surface morphology analysis were examined on a SUPPA 55 scanning electron microscopy (SEM) system (Zeiss, Germany) and a high resolution transmission electron microscope (HR-TEM) of FEI Tecnai G20 (FEI Corp., USA) with an acceleration voltage of 200 kV. The crystalline phase of the material was identified using an X-ray diffractometer (XRD; D/max-2500VPC, Rigaku, Japan) with Ni-filtered Cu-Ka radiation. Fourier transform infrared (FT-IR) spectra were taken on a NEXUS 670 FT-IR Spectrometer (Madison, WI, USA). Magnetic property of the material was investigated using a vibrating sample magnetometer (LDJ9600). Elemental compositions and contents of these materials were determined using energy-dispersive spectroscope (EDS, S-3000N Hitachi, Japan). Nitrogen adsorption–desorption isotherms were measured at 77 K on a Micromeritics ASAP-2020 (USA) after the sample was vacuum-dried at 30°C for at least 12 h. The specific surface area was calculated with MultiPoint Brunauer–Emmett–Teller (BET) method, and total pore volume and pore diameter were obtained by Barrett–Joyner–Halenda method. Raman spectra of the prepared material were recorded with a laser excitation wavelength of 514 nm on a Jobin-Yvon LabRam spectrometer (HR-800, France).

2.4. Batch adsorption experiments

The total volume of solution was 25 mL containing 0.1 g L^{-1} sorbent, and the solution pH was adjusted to designed value with HCl and NaOH solution. To carry out the adsorption isotherms study, the concentrations of methyl green, neutral red and congo red were set in the range of 50–400, 50–400 and 20–260 mg L^{-1}, respectively. The adsorption dynamics was carried out with initial concentrations of methyl green, neutral red and congo red at 50, 40 and 40 mg L^{-1}, respectively, and 10 mL of solution were taken for determination at different time intervals. Thermodynamic experiments were also conducted at the temperature of 20°C, 30°C and 40°C, and the initial concentrations of methyl green, neutral red, and congo red were 40, 60, 60 mg L^{-1}. The practical application of the MMC material was investigated through removal of dyes from tap water, lake water and sea water. All the experiments were shaken for 24 h at 30°C at a water-bath oscillator in order to reach the adsorption equilibrium completely.

After adsorption, the MMC sorbents were separated from aqueous solution with a magnet, and the supernatant was taken for analysis. An UV-Vis spectrophotometer (UV-2550, Shimadzu, Japan) was used to determine the concentrations of target dyes.

2.5. Collection of natural water samples

Three types of environmental water samples were collected from different district of Yantai, Shandong province, as matrix for dye adsorption. Tap water sample was taken from our lab, and lake water sample was obtained from Ruzi lake in our campus. Sea water sample was collected from coastal water of the Huanghai Sea. All samples were collected in polypropylene bottles and suspended particles were removed through filtration.

3. Results and discussion

3.1. Characterization of materials

The surface morphology of SBA-15 and MMC material were studied by SEM and TEM, and the results are shown in Fig. 2. The SEM image in Fig. 2(a) shows that the morphology of SBA-15 was linked with rod particles possessing the features of hexagon section. The TEM image of SBA-15 in Fig. 2(b) shows a typical mesochannel. As shown in Fig. 2(c), mesoporous structure was observed obviously from SEM image of MMC. The TEM image of MMC in Fig. 2(d) shows that fine particles of Fe_3O_4 with nearly spherical shape were distributed uniformly in MMC. Additionally, to investigate the composition of samples in every reaction stage, element analysis was carried out by EDS and the results are shown in Fig. 3. As can be seen from Fig. 3(a), the EDS spectrum of SBA-15 shows strong peaks of silica and oxygen, and the contents were 58.19 wt% and 41.81 wt%, respectively. After PDA and Fe^{3+} were filled into the pore channel of SBA-15, the spectrum in Fig. 3(b) not only shows peak of silica, but

also obvious peaks of carbon and iron, indicating carbon precursor and iron source were introduced successfully. Fig. 3(c) is the spectrum of calcined material under inert atmosphere, and the peak of nitrogen presented remarkable reduction, while others showed no obvious change. Fig. 3(d) illustrates the spectrum of the material that SBA-15 template was dissolved, the peak of carbon and iron presented remarkable increase, while the peak of silica disappeared, and the peak of oxygen decreased obviously, demonstrating that the final product was the combination of carbon material and iron composition.

The FT-IR spectra of SBA-15, PDA-Fe^{3+}/SBA-15, C-Fe/SBA-15 and MMC samples are shown in Fig. 4. The sharp bands at 1,083; 794 and 462 cm^{-1} on spectrum of SBA-15 were all ascribed to the Si–O–Si bands [45]. As shown in the spectrum

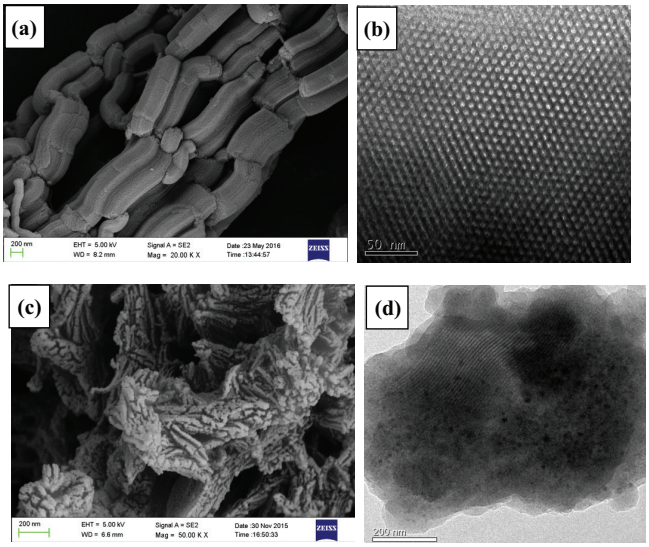

Fig. 2. SEM images of SBA-15 (a) and MMC material (c), TEM images of SBA-15 (b) and MMC (d) materials.

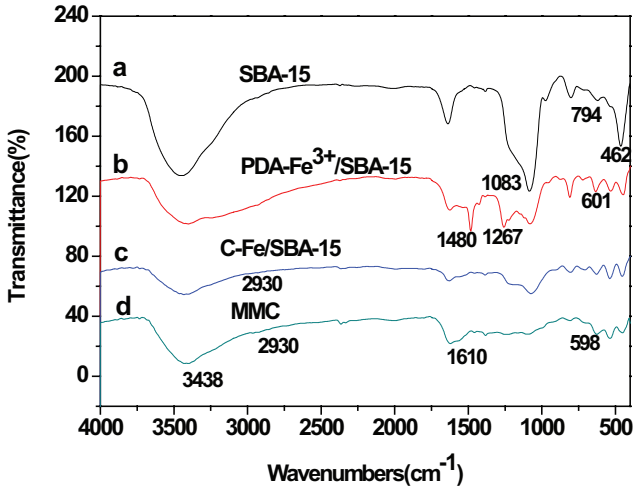

Fig. 4. FT-IR spectra of SBA-15 (a), PDA-Fe^{3+}/SBA-15 (b), C-Fe/SBA-15 (c) and MMC (d).

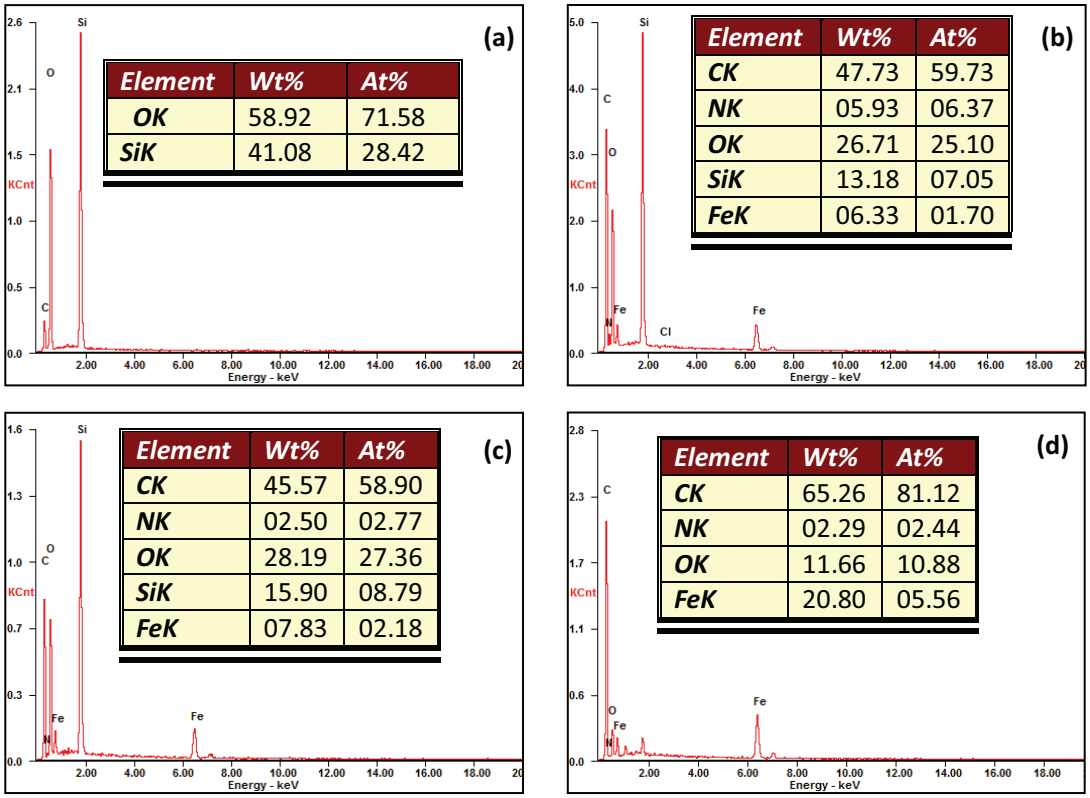

Fig. 3. EDS of SBA-15 (a), PDA-Fe^{3+}/SBA-15 (b), C-Fe/SBA-15 (c) and MMC (d).

of PDA-Fe^{3+}/SBA-15, the peaks at 1,480 and 1,267 cm^{-1} should be assigned to the presence of PDA [46], and the band near 600 cm^{-1} was ascribed to the Fe–O band [30]. All these revealed that PDA and Fe^{3+} were filled into the pore channel of SBA-15. After calcination under high temperature, the characteristic peak of polydopamine decreasing, and the weak peak near 2,930 cm^{-1} indicated the presence of C–C in the carbon, indicating polydopamine was almost carbonized. In spectrum of MMC, characteristic peaks of SBA-15 were disappeared, suggesting that silica template was removed completely and MMC was prepared successfully. It should also be noted that the peaks at 1,610 and 3,438 cm^{-1} shown in all spectra represented adsorbed water and hydroxyl groups [36].

N_2 adsorption/desorption isotherms of both SBA-15 and MMC shown in Fig. 5 exhibited a type IV isotherm with a H_1 hysteresis loop, which corresponded with the typical characteristic of mesoporous materials [47]. BET surface areas of the SBA-15 and MMC were 744 and 480 $cm^2\ g^{-1}$, and total pore volumes were 0.97 and 0.47 $cm^3\ g^{-1}$. As shown in the inset of Fig. 5, the pore diameter distribution of the SBA-15 and the MMC showed sharp peaks at 6.47 and 3.87 nm.

The XRD pattern of MMC is shown in Fig. 6(a). The MMC diffraction peaks at 30.10°, 35.45°, 43.08°, 53.45°, 56.98°, 62.57° and 74.02° confirmed the formation of the Fe_3O_4 particles (JCPDS No. 65-3107). Other peaks at 24.13°, 33.12°, 43.42° and 49.48° were diffraction peaks of the Fe_2O_3 particles (JCPDS No. 24-0072). It indicated that a part of Fe_3O_4 changed to Fe_2O_3 at elevated temperature. To further explore the degree of the graphitization of MMC, Raman spectrum of MMC was analyzed and the result is shown in Fig. 6(b). As we could see, two intense bands at 1,344 and 1,589 cm^{-1} were in agreement with the D and G bands, respectively. The value of I_D/I_G was 1.1, which confirmed that more lattice defects were presented in the surface of the MMC, resulting in a typical disordered structure of graphite.

Fig. 6(c) shows the magnetization hysteresis loops of MMC. There was a slight hysteresis in the hysteresis loops of MMC, and the measured remanence value and coercivity were 5.34 $emu\cdot g^{-1}$ and 147 Oe, respectively. The maximal saturation magnetization of MMC was 19.90 $emu\cdot g^{-1}$. This phenomenon demonstrated that phase transition happened for magnetic nanoparticles under high temperature. It also

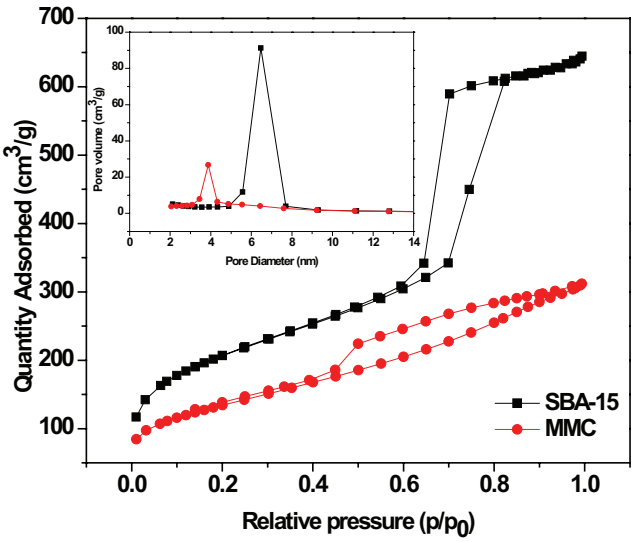

Fig. 5. N_2 adsorption/desorption isotherms and pore size distribution (inset graph) of both SBA-15 and MMC.

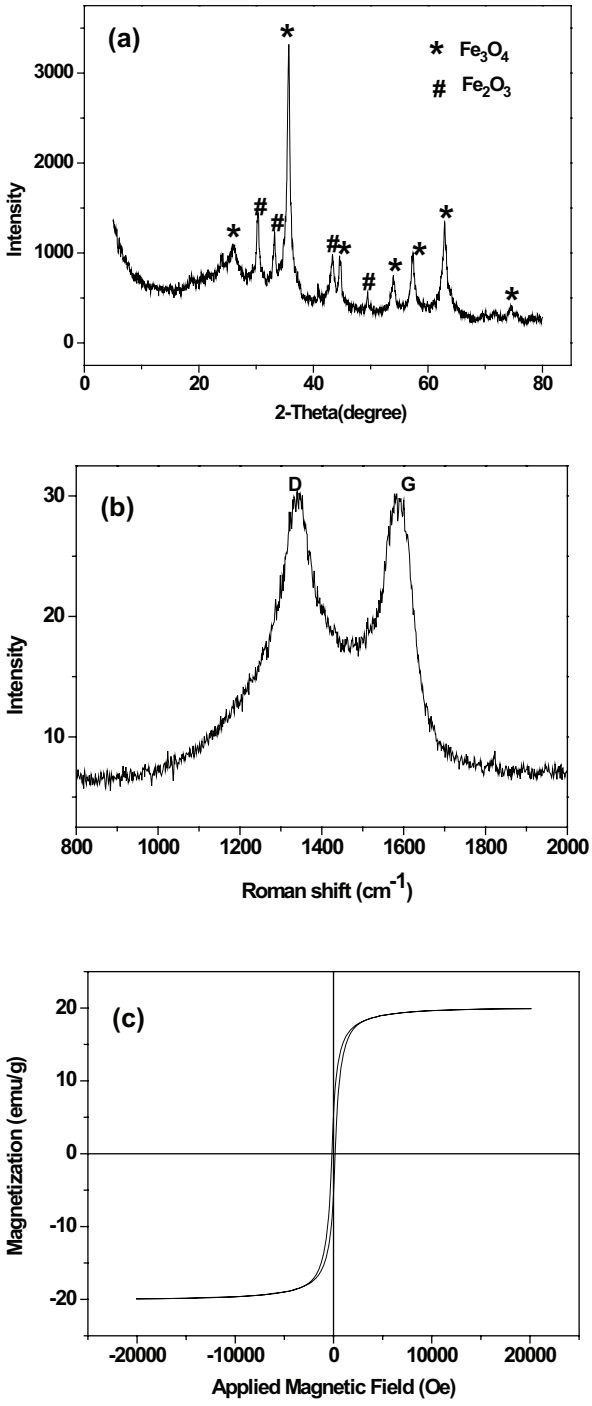

Fig. 6. XRD pattern (a), Raman spectra (b) and magnetization hysteresis loops (c) of the MMC material.

suggested that the MMC possessed excellent paramagnetism and high saturation magnetization, which was beneficial to its separation and collection from solution.

3.2. Effect of solution pH and ionic strength on dyes adsorption

Solution pH was adjusted in the range of 3–10 to investigate the effect of pH on dyes adsorption, and the initial concentrations of Congo red, neutral red and methyl green were set at 20, 30, 20 mg·L^{-1}, respectively. The results are shown in Fig 7(a). With the increase of pH, adsorption capacity of cationic dye neutral red and methyl green increased quickly, and then gradually declined after attaining the peak. For acidic dye congo red, with the increase of pH, adsorption capacity gradually increased at first, and no significant change was observed with pH in the range of 5–10. The results could be explained by electrostatic interactions between dyes and surface charge of sorbent. For cationic dye, the decrease of adsorption capacity might be attributed to protonation effect of the MMC material in the acidic condition, the adsorption of cationic dye was prevented by the positive charged surface of the MMC. With the increase of solution pH, ionizable surface sites of the MMC material increased, and surface potential of the MMC turned into negative, so the electrostatic attraction enhanced the adsorption capacity. On the contrary, for anionic dye, when pH was less than 4, the relatively low adsorption capacity might be resulted from the difficult combination between congo red and the sorbent. The large adsorption capacity obtained at pH 4, this was because that the amino group in congo red molecule could neutralize a small amount of protons, and with the increase of pH, adsorption capacity remained nearly unchanged. Therefore, pH values of 4, 7 and 7 were recommended in further experiments for congo red, neutral red and methyl green, respectively.

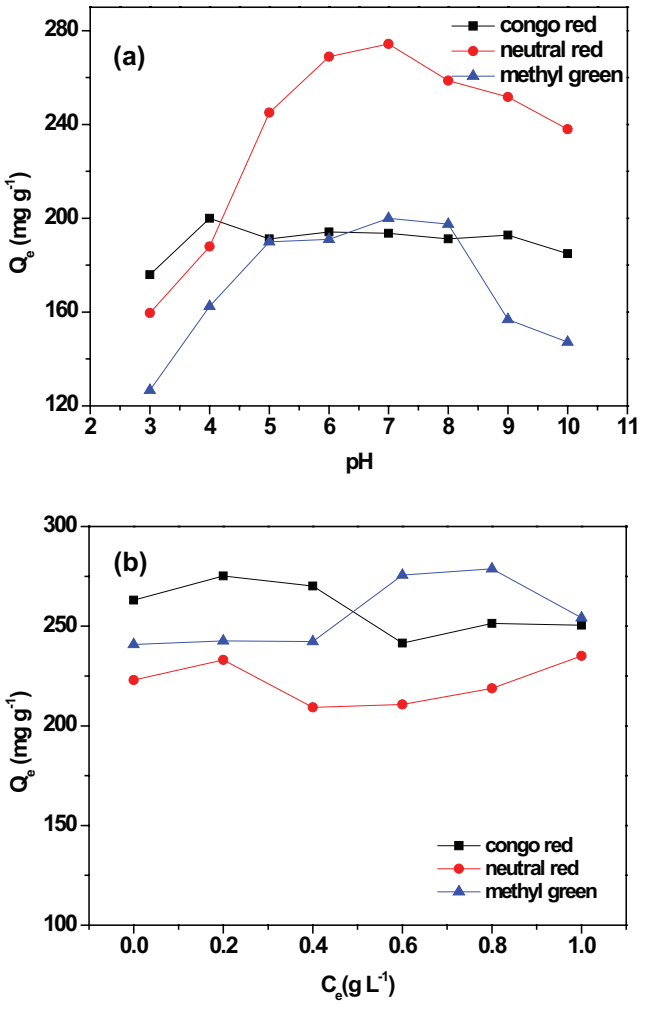

Fig. 7. Effect of solution pH (a) and ionic strength (b) on the adsorption of dyes on the MMC sorbent.

The effect of ionic strength on adsorption was examined by adjusting the salinity of solution with NaCl in the range of 0–1 g L^{-1}. The results in Fig. 7(b) indicate that the removal efficiency of the dyes was independent of the ionic strength.

3.3. Adsorption isotherms at different temperatures

The adsorption isotherms of the MMC material for the three dyes were carried out at 20°C, 30°C, 40°C and the initial concentrations of congo red, neutral red and methyl green were set at 20–260, 50–400 and 50–400 mg L^{-1}, respectively. Fig. 8 shows the equilibrium adsorption curves. The adsorption capacity enhanced rapidly at beginning, and then reached a platform with the increase of initial concentration of dyes. It could be observed that the MMC exhibited ultrahigh adsorption capacity for these dyes, which resulted from large specific surface area and abundant adsorption sites of MMC. The adsorption data were fitted with Langmuir, Freundlich, and Temkin models, and their linear equations are shown as follows:

$$\frac{C_e}{q_e} = \frac{1}{\theta b} + \frac{C_e}{\theta} \tag{1}$$

$$\log q_e = \log K_F + \frac{1}{n}\log C_e \tag{2}$$

$$q_e = a + b\log C_e \tag{3}$$

where C_e (mg L^{-1}) and q_e (mg g^{-1}) are equilibrium concentration and equilibrium adsorption capacity; θ (mg g^{-1}) is maximum adsorption capacity and b (L mg^{-1}) is equilibrium adsorption constant. The maximum adsorption capacity (θ) can be calculated from the slope of the linear plot of C_e/q_e vs. C_e. K_F (mL$^{1/n}$ μg$^{1-1/n}$) and n is the Freundlich constants. The value of n and K_F can be obtained from slope of linear plot of $\log q_e$ vs. $\log C_e$. The Temkin constants a and b can be calculated from the slope and intercept of the linear plot of q_e vs. $\log C_e$. Table 1 shows the fitting parameters of Langmuir, Freundlich, and Temkin models. The correlation coefficients (R^2) of Langmuir, Freundlich and Temkin models were in the range of 0.978–0.994, 0.960–0.985 and 0.900–0.992, respectively. The Langmuir model was more suitable to fit the adsorption data than Freundlich and Temkin models. The fitting lines of Langmuir isotherm model were shown in the inset graph of Fig. 8, and they exhibited good linear correlation. The maximum adsorption capacity of congo red, neutral red, and

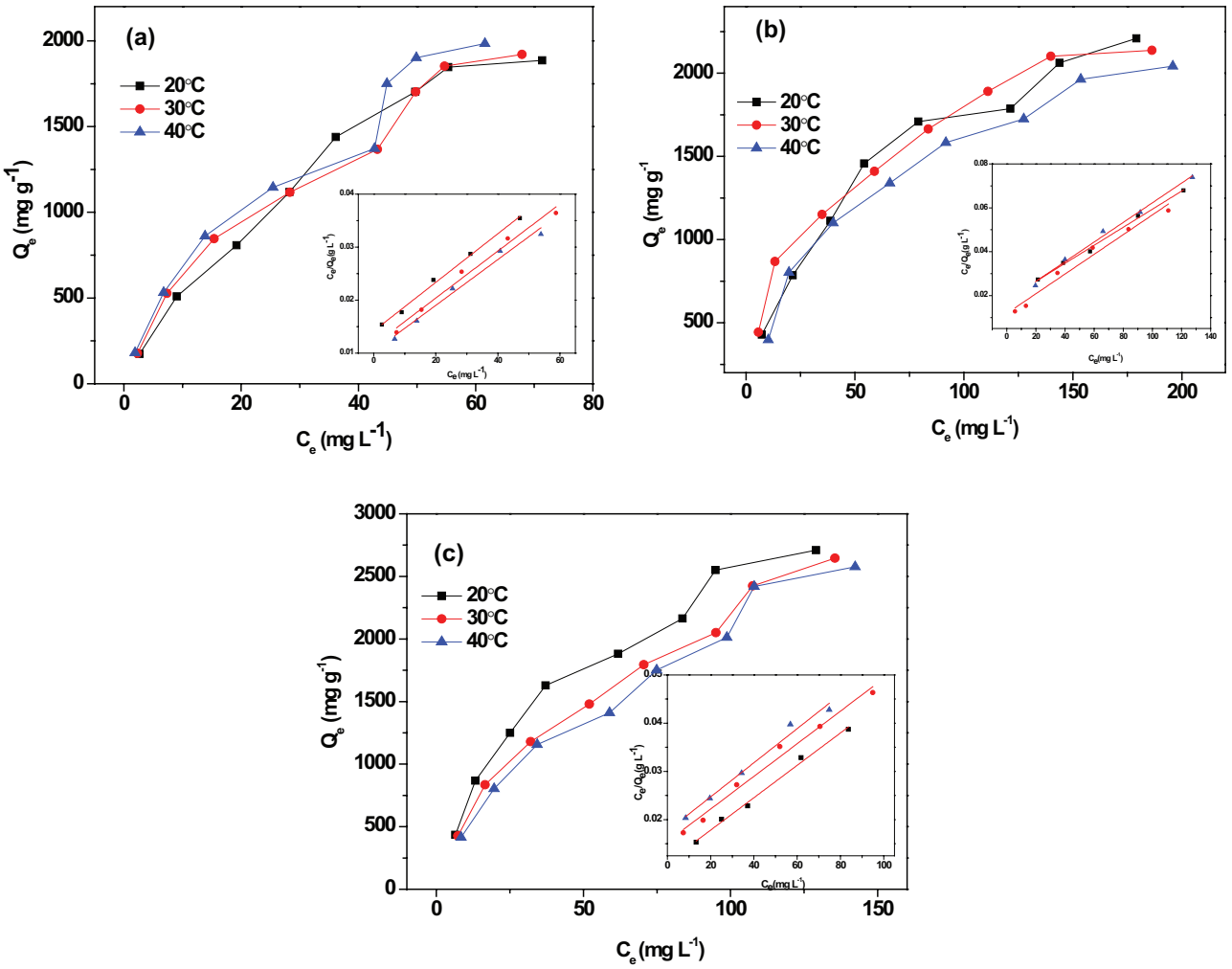

Fig. 8. Adsorption isotherms and fitting curves of Langmuir isotherm models of congo red (a), neutral red (b) and methyl green (c) on the MMC sorbent.

Table 1
Langmuir, Freundlich, and Temkin isotherms parameters for dye adsorption on the MMC material

Pollutants	Temperature (°C)	Langmuir model			Freundlich model			Temkin model		
		θ (mg·g^{-1})	b (g·mL^{-1})	R^2	K_F (mL$^{1/n}$·μg$^{1-1/n}$)	n	R^2	a	b	R^2
Congo red	20	2181.1	0.032	0.9943	90.1	1.337	0.9888	–603.3	1291.5	0.9113
	30	2256.0	0.037	0.9823	114.8	1.458	0.9791	–469.4	1229.4	0.9253
	40	2315.4	0.041	0.9797	133.0	1.500	0.9681	–337.3	1193.7	0.9000
Neutral red	20	2431.6	0.022	0.9946	165.9	1.952	0.9774	–837.2	1311.0	0.9648
	30	2226.1	0.037	0.9726	239.1	2.294	0.9684	–472.9	1138.1	0.9711
	40	2235.1	0.025	0.9908	145.2	1.925	0.9483	–893.5	1265.4	0.9923
Methyl green	20	2927.1	0.030	0.9920	126.8	2.033	0.9739	–1075	1738.4	0.9710
	30	2916.8	0.022	0.9833	137.2	1.646	0.9800	–1174	1674.9	0.9304
	40	2827.6	0.020	0.9787	161.4	1.507	0.9749	–1370	1731.9	0.9169

methyl green calculated from Langmuir model were 2,315.4; 2,431.6 and 2,956.8 mg g^{-1}, respectively. As a comparison, the maximum adsorption capacity of congo red, neutral red, and methyl green on MC calculated from Langmuir model were 3,321.2; 3,506.9 and 2,874.4 mg g^{-1}, respectively (figure not shown). The adsorption capacity of congo red and neutral red were higher than on MMC, and that of methyl green was similar with on MMC. The results indicated that the valid

adsorption sites were mainly from MC material, and the addition of Fe_3O_4 reduced the adsorption sites, thus leading to the decrease of the adsorption capacity. Nevertheless, the introduction of Fe_3O_4 facilitated the separation of sorbents with a magnet for regeneration. The interactions between organic pollutants and carbonaceous materials include hydrophobic interactions, π – π stacking, electrostatic interactions, and hydrogen bonds [48]. The nitrogen in PDA would result in MMC materials containing abundant N atoms, and the strong electronegativity of nitrogen decreased the electron density of the graphite surface, which enhanced π-electron accepting capacity of the N-doped material. The aromatic rings of dye molecules are π-electron rich and generally considered as π-donor. Thus, π–π electron donor–accepter interaction enhanced the adsorbability of MMC for dye pollutants [49]. The high adsorption capacity was mainly attributed to the existence of ordered mesoporous structure and the electron-donating effect of the incorporated nitrogen-containing functional groups [50]. Thus, the ultrahigh adsorption capacity suggested that the present MMC material possessed great potential for purification of dye wastewater.

3.4. Adsorption kinetics

The adsorption kinetics of dyes on the MMC material was performed at an initial concentration of 40, 40 and 50 mg L^{-1} for congo red, neutral red and methyl green, respectively. Fig. 9 shows the uptake rate of dyes at different temperature. It could be seen that the adsorption capacity was enhanced quickly in the initial time, and then slowed down, and finally adsorption capacity no longer changed. The initial fast adsorption resulted from the high concentrations of dyes and plenty of adsorption sites on the surface of material, and the decrease of adsorption sites and diffusion of dye molecules into pore of MMC lead to subsequent slow adsorption speed. Moreover, adsorption capacity of congo red at high temperature was higher than at low temperature. On the contrary, low temperature was advantageous to the adsorption of neutral red and methyl green. According to the results, the contact time of 8, 8 and 10 h were sufficient to achieve balance for congo red, neutral red and methyl green, respectively. In order to investigate the adsorption rate of dyes on the MMC material, the kinetic data were analyzed with the pseudo-second order kinetic model, and linear equation of the model is as follows:

$$\frac{t}{q_t} = \frac{1}{kq_e^2} + \frac{1}{q_e}t \tag{4}$$

where k (g mg^{-1} min^{-1}) is the adsorption rate constant, q_t (mg g^{-1}) and q_e (mg g^{-1}) are the adsorption capacity at certain time and equilibrium adsorption capacity, and h (mg g^{-1} min^{-1}) is the initial adsorption rate, which can be defined as follows:

$$h = kq_e^2 \quad (t \to 0) \tag{5}$$

k and h can be obtained from the slope and intercept of plot of t/q_t vs. t, and the results are presented in Table 2. As shown in the inset of Fig. 9, the fitting curves of pseudo-second order kinetic model showed good linear relationship with R^2 over 0.999. The MMC sorbent showed high adsorption efficiency and fast adsorption rate for dye pollutants.

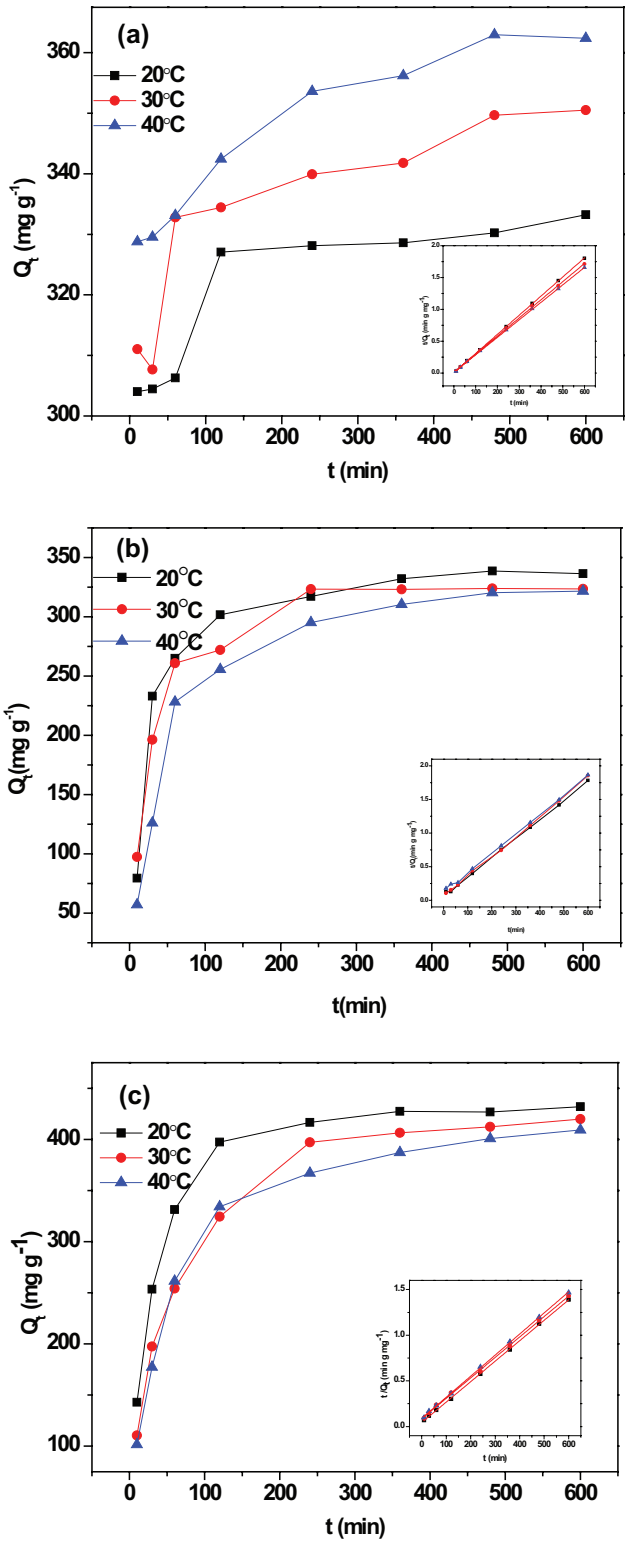

Fig. 9. Adsorption kinetics data and curves of pseudo-second-order kinetic fitting of congo red (a), neutral red (b) and methyl green (c) on the MMC sorbent.

3.5. Adsorption thermodynamics

Furthermore, adsorption thermodynamics could be discussed based on the adsorption data at different temperature (20°C, 30°C and 40°C). The thermodynamic equations are given as follows:

$$K_C = \frac{q_e}{C_e} \tag{6}$$

$$\ln K_c = \frac{\Delta S^\circ}{R} - \frac{\Delta H^\circ}{RT} \tag{7}$$

$$\Delta G^\circ = \Delta H^\circ - T\Delta S^\circ \tag{8}$$

where q_e (mg g^{-1}) and C_e (mg L^{-1}) are equilibrium adsorption capacity and equilibrium concentration; K_c and T are solid–liquid distribution coefficient and thermodynamic temperature, and R is gas constant (8.314 J mol^{-1} K^{-1}). $\Delta H°$ (kJ mol^{-1}), $\Delta S°$ (J mol^{-1} K^{-1}) and $\Delta G°$ (kJ mol^{-1}) are change of enthalpy, entropy and Gibbs free energy under standard condition, respectively. The value of $\Delta H°$ and $\Delta S°$ can be calculated from slope and intercept of linear fitting of $\ln K_c$ vs. $1/T$, and that of $\Delta G°$ was obtained from Eq. (7). Table 3 lists the equilibrium adsorption data and thermodynamic parameters, and some conclusions could be drawn as follows: (1) adsorption capacity of congo red on MMC increased with the rise of the temperature, indicating an endothermic process. The values of $\Delta H°$ and $\Delta S°$ were 32.70 kJ mol^{-1} and 143.32 J mol^{-1} K^{-1}, respectively. The negative value of $\Delta G°$ confirmed a spontaneous process of the adsorption; (2) With the decrease of temperature, the adsorption capability for neutral red and methyl green on MMC increased slightly, indicating an exothermic process in nature. This was also confirmed by the negative $\Delta H°$ values. The negative $\Delta S°$ values confirmed a chaotic degree decreasing process of the adsorption. The negative values of $\Delta G°$ also suggested the spontaneous process of the adsorption.

Table 2
Pseudo-second-order rate constants for congo red, neutral red and methyl green adsorption on the MMC sorbent

Pollutants	Temperature (°C)	k (g·mg^{-1}·min^{-1})	h (mg·g^{-1}·min^{-1})	R^2
Congo red	20	9.12×10^{-4}	101.41	0.9999
	30	6.02×10^{-4}	74.68	0.9997
	40	5.61×10^{-4}	74.73	0.9998
Neutral red	20	1.26×10^{-4}	15.56	0.9991
	30	1.41×10^{-4}	16.14	0.9991
	40	6.45×10^{-5}	7.84	0.9989
Methyl green	20	1.13×10^{-4}	22.71	0.9997
	30	5.91×10^{-5}	11.77	0.9991
	40	5.94×10^{-5}	11.13	0.9996

3.6. Reusability of MMC and environmental significance

The reusability of the adsorbent is of great importance for improving adsorption efficiency and economic feasibility. To investigate the reusability of MMC, the dye-loaded MMC was separated with a magnet and then 10 mL of ethanol were added for desorption. After vibration for 1 h, the MMC was separated and rinsed with deionized water, and then it was used in the next adsorption/desorption cycles. As shown in Fig. 10, the adsorption capacity decreased gradually with increasing recycle times, which resulted from part irreversible adsorption of the dye on MMC and unavoidable loss of the sorbent during the recycle process. However, after five times of recycle, the MMC still maintained quite high adsorption capacity (over 400 mg g^{-1}). The high adsorption efficiency together with easy separation and good regeneration made the MMC promising sorbent for removal of organic dyes from aqueous solution.

Tap water, lake water and seawater were used as matrix to test the practical application of MMC material for removal of dye pollutants from natural water. Fig. 11 shows the

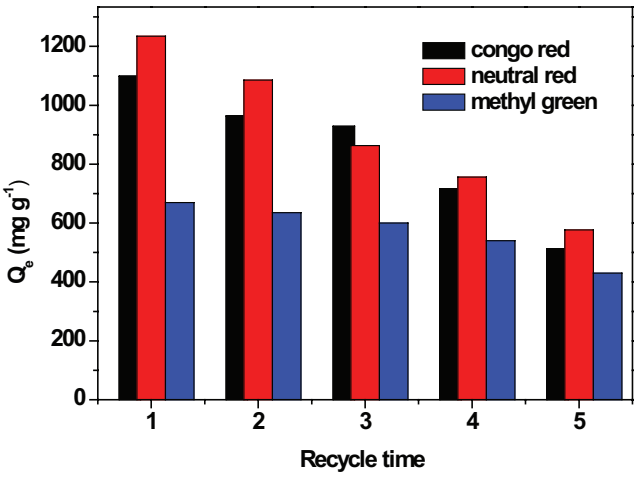

Fig. 10. Reusability of MMC for dye adsorption.

Table 3
Thermodynamic parameters for adsorption of dyes onto MMC sorbent

Dyes	C_0 (mg L^{-1})	C_e (mg L^{-1})			$\Delta H°$ (kJ mol^{-1})	$\Delta S°$ (J mol^{-1} K^{-1})	$\Delta G°$ (kJ mol^{-1})		
		At 293 K	At 303 K	At 313 K			At 293 K	At 303 K	At 313 K
Congo red	60	10.31	8.24	4.84	32.70	143.32	–9.29	–10.72	–12.16
Neutral red	60	9.57	11.87	12.93	–14.14	–15.55	–9.58	–9.43	–9.27
Methyl green	40	3.25	4.28	6.79	–31.83	–68.99	–11.61	–10.92	–10.23

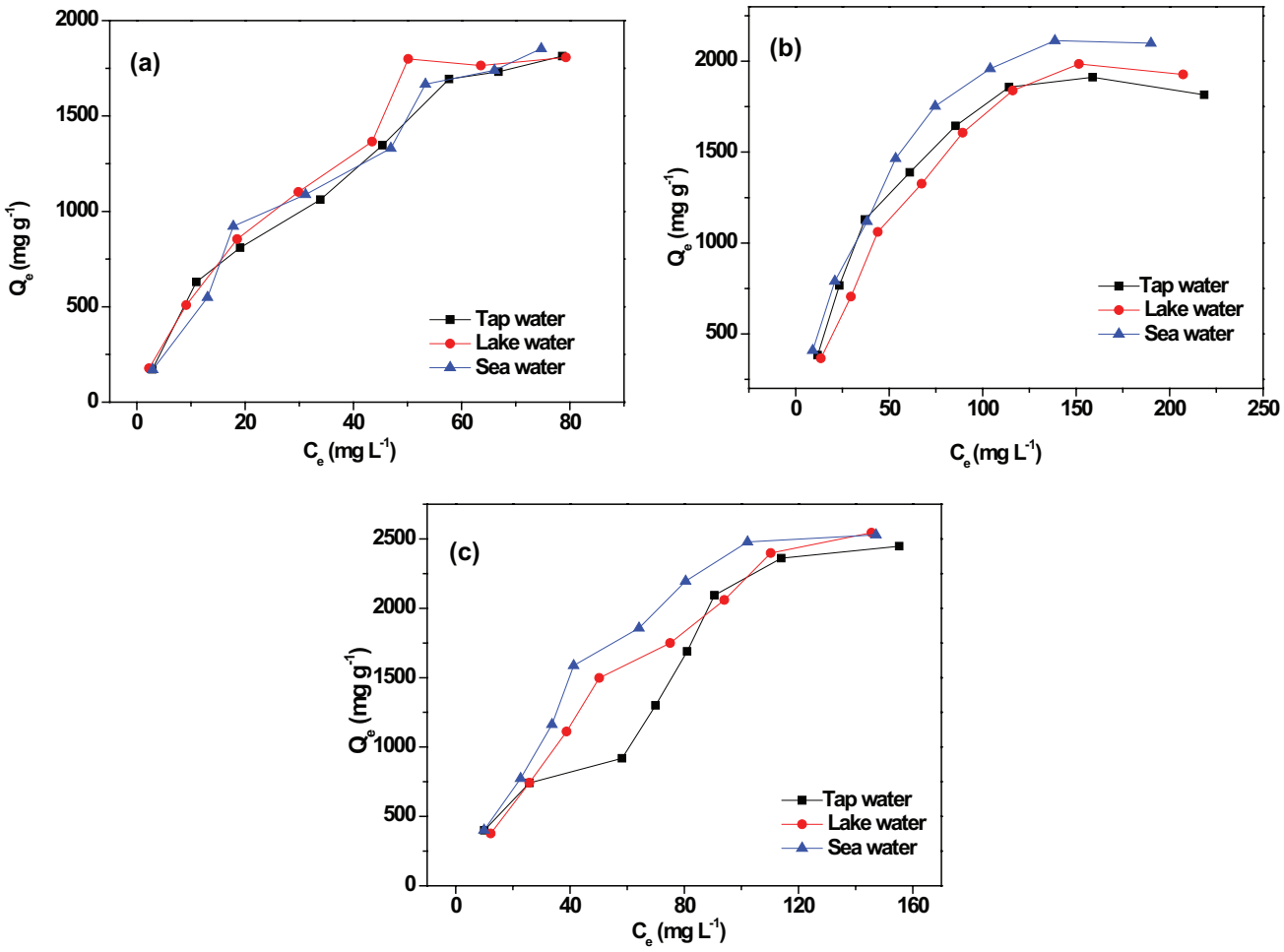

Fig. 11. Adsorption isotherms of (a) congo red, (b) neutral red, (c) methyl green on the MMC sorbent from the natural water samples.

Table 4
Langmuir and Freundlich isotherm parameters for dye adsorption on MMC material with the natural water at 30°C

Pollutants	Water matrix	Langmuir model			Freundlich model		
		θ (mg·g^{-1})	b (g·mL^{-1})	R^2	K_F (mL$^{1/n}$·μg$^{1-1/n}$)	n	R^2
Congo red	Tap water	2,258.2	0.030	0.9592	94.4	1.435	0.9322
	Lake water	2,218.1	0.034	0.9696	109.5	1.487	0.9450
	Sea water	2,297.9	0.031	0.9844	92.2	1.402	0.9805
Neutral red	Tap water	2,318.6	0.023	0.9692	134.9	1.874	0.8749
	Lake water	2,460.5	0.021	0.9576	81.9	1.561	0.9348
	Sea water	2,533.9	0.029	0.9880	139.0	1.791	0.9444
Methyl green	Tap water	2,678.2	0.015	0.8518	80.8	1.387	0.7027
	Lake water	2,812.7	0.013	0.8932	122.3	1.676	0.7285
	Sea water	2,888.6	0.016	0.9970	90.1	1.489	0.9884

adsorption data, and fitting parameters of Langmuir and Freundlich models are given in Table 4. The Langmuir model fit adsorption data better than Freundlich model. Compared with pure water, the saturated adsorption capacity showed no obvious decrease in natural water, indicating that the MMC material possessed great potential for purification of dye wastewater.

4. Conclusion

The dopamine could auto-polymerize on the pore channel of SBA-15 as well as Fe^{3+} coordination with polydopamine, and carbonization of polydopamine and conversion of Fe^{3+} to magnetic nanoparticles occurred simultaneously under high-temperature calcination. After SBA-15 template was

dissolved, MMC based on polydopamine was synthesized successfully. The obtained MMC showed a high BET surface area and uniform pore size. The adsorption of three dyes on the prepared MMC fit Langmuir model, and the maximum adsorption capability were all more than 2,000 mg g^{-1}, presenting attractive potential for removal of dye pollutants. In addition, the MMC also showed high adsorption capacity for dye pollutants from natural water matrix. The study not only prepared a high-efficient magnetic sorbent for dyes but also provided a new idea for synthesis of magnetic composites based on auto-polymerization materials.

Acknowledgments

This work was jointly supported by the National Natural Science Foundation of China (21207059); the Natural Science Foundation of Shandong Province (ZR2011BQ012, ZR2016BM27, ZR2017PB006).

References

[1] N.D. Petkovich, A. Stein, Controlling macro- and mesostructures with hierarchical porosity through combined hard and soft templating, Chem. Soc. Rev., 42 (2013) 3721–3739.
[2] W. Li, D. Zhao, An overview of the synthesis of ordered mesoporous materials, Chem. Commun., 49 (2013) 943–946.
[3] W. Li, J. Liu, D. Zhao, Mesoporous materials for energy conversion and storage devices, Nature Rev. Mater., 1 (2016) 16023.
[4] Y.R. Lin, H. Teng, Mesoporous carbons from waste tire char and their application in wastewater discoloration, Microporous Mesoporous Mater., 54 (2002) 167–174.
[5] A. Vinu, K.Z. Hossain, G.S. Kumar, K. Ariga, Adsorption of L-histidine over mesoporous carbon molecular sieves, Carbon, 44 (2006) 530–536.
[6] L.J. Kennedy, J.J. Vijaya, K. Kayalvizhi, G. Sekaran, Adsorption of phenol from aqueous solutions using mesoporous carbon prepared by two-stage process, Chem. Eng. J., 132 (2007) 279–287.
[7] A. Chen, Y. Li, Y. Yu, Y. Yu, Y. Li, Rapid and Facile Synthesis of Rod-Like Ordered Mesoporous Carbon Material for Dye Adsorption from Aqueous Solution, Aust. J. Chem., 69 (2016) 785–789.
[8] X. Sheng, N. Daems, B. Geboes, M. Kurttepeli, S. Bals, T. Breugelmans, A. Hubin, I.F.J. Vankelecom, P.P. Pescarmona, N-doped ordered mesoporous carbons prepared by a two-step nanocasting strategy as highly active and selective electrocatalysts for the reduction of O_2 to H_2O_2, Appl. Catal. B-Environ., 176–177 (2015) 212–224.
[9] J.M. Nhut, L. Pesant, J.P. Tessonnier, G. Winé, J. Guille, C. Pham-Huu, M.J. Ledoux, Mesoporous carbon nanotubes for use as support in catalysis and as nanosized reactors for one-dimensional inorganic material synthesis, Appl. Catal. A-General, 254 (2003) 345–363.
[10] Y. Liang, H. Liu, Z. Li, R. Fu, D. Wu, In situ polydopamine coating-directed synthesis of nitrogen-doped ordered nanoporous carbons with superior performance in supercapacitors, J. Mater. Chem. A, 1 (2013) 15207.
[11] H. Chang, H.J. Sang, C. Pak, Synthesis and characterization of mesoporous carbon for fuel cell applications, J. Mater. Chem., 53 (2007) 301–312.
[12] J. Lee, S. Yoon, T. Hyeon, S.M. Oh, K.B. Kim, Synthesis of a new mesoporous carbon and its application to electrochemical double-layer capacitors, Chem. Commun., 21 (1999) 2177–2178.
[13] Y. Meng, D. Gu, F. Zhang, Y. Shi, H. Yang, Z. Li, C. Yu, B. Tu, D. Zhao, Ordered mesoporous polymers and homologous carbon frameworks: amphiphilic surfactant templating and direct transformation, Angew. Chem. Int. Ed., 44 (2005) 7053–7059.
[14] F. Zhang, Y. Meng, D. Gu, Yan, C. Yu, B. Tu, D. Zhao, A facile aqueous route to synthesize highly ordered mesoporous polymers and carbon frameworks with Ia3d bicontinuous cubic structure, J. Am. Chem. Soc., 127 (2005) 13508–13509.
[15] M. Xie, H. Dong, D. Zhang, X. Guo, W. Ding, Simple synthesis of highly ordered mesoporous carbon by self-assembly of phenol–formaldehyde and block copolymers under designed aqueous basic/acidic conditions, Carbon, 49 (2011) 2459–2464.
[16] D. Liu, J.-H. Lei, L.-P. Guo, D. Qu, Y. Li, B.-L. Su, One-pot aqueous route to synthesize highly ordered cubic and hexagonal mesoporous carbons from resorcinol and hexamine, Carbon, 50 (2012) 476–487.
[17] J.-S. Lee, S.H. Joo, R. Ryoo, Synthesis of mesoporous silicas of controlled pore wall thickness and their replication to ordered nanoporous carbons with various pore diameters, J. Am. Chem. Soc., 124 (2002) 1156–1157.
[18] F. Li, K.-Y. Chan, H. Yung, Carbonization over PFA-protected dispersed platinum: an effective route to synthesize high performance mesoporous-carbon supported Pt electrocatalysts, J. Mater. Chem., 21 (2011) 12139.
[19] G. Zolfaghari, A. Esmaili-Sari, M. Anbia, H. Younesi, S. Amirmahmoodi, A. Ghafari-Nazari, Taguchi optimization approach for Pb(II) and Hg(II) removal from aqueous solutions using modified mesoporous carbon, J. Hazard. Mater., 192 (2011) 1046–1055.
[20] D. Zhao, J. Feng, Q. Huo, N. Melosh, G.H. Fredrickson, B.F. Chmelka, G.D. Stucky, Triblock copolymer syntheses of mesoporous silica with periodic 50 to 300 angstrom pores, Science, 279 (1998) 548–552.
[21] K. Xia, Q. Gao, C. Wu, S. Song, M. Ruan, Activation, characterization and hydrogen storage properties of the mesoporous carbon CMK-3, Carbon, 45 (2007) 1989–1996.
[22] X. Xiao, F. Zhang, Z. Feng, S. Deng, Y. Wang, Adsorptive removal and kinetics of methylene blue from aqueous solution using NiO/MCM-41 composite, Physica E, 65 (2015) 4–12.
[23] T.W. Kim, Characterization of mesoporous carbons synthesized with SBA-16 silica template, J. Mater. Chem., 15 (2005) 1560–1571.
[24] W. Xing, S.Z. Qiao, R.G. Ding, F. Li, G.Q. Lu, Z.F. Yan, H.M. Cheng, Superior electric double layer capacitors using ordered mesoporous carbons, Carbon, 44 (2006) 216–224.
[25] X. Peng, X. Hu, D. Fu, F.L.Y. Lam, Adsorption removal of acid black 1 from aqueous solution using ordered mesoporous carbon, Appl. Surf. Sci., 294 (2014) 71–80.
[26] F.A. Casado-Carmona, M.D.C. Alcudia-León, R. Lucena, S. Cárdenas, M. Valcárcel, Magnetic nanoparticles coated with ionic liquid for the extraction of endocrine disrupting compounds from waters, Microchem. J., 128 (2016) 347–353.
[27] R. Verma, A. Asthana, A.K. Singh, S. Prasad, M.A.B.H. Susan, Novel glycine-functionalized magnetic nanoparticles entrapped calcium alginate beads for effective removal of lead, Microchem. J., 130 (2016) 168–178.
[28] Z. Xiao, M. Yuan, B. Yang, Z. Liu, J. Huang, D. Sun, Plant-mediated synthesis of highly active iron nanoparticles for Cr (VI) removal: investigation of the leading biomolecules, Chemosphere, 150 (2016) 357–364.
[29] H. Luo, S. Zhang, X. Li, X. Liu, Q. Xu, J. Liu, Z. Wang, Tannic acid modified Fe_3O_4 core–shell nanoparticles for adsorption of Pb^{2+} and Hg^{2+}, J. Taiwan Inst. Chem. Eng., 72 (2017) 163–170.
[30] S. Zhang, Y. Zhang, G. Bi, J. Liu, Z. Wang, Q. Xu, H. Xu, X. Li, Mussel-inspired polydopamine biopolymer decorated with magnetic nanoparticles for multiple pollutants removal, J. Hazard. Mater., 270 (2014) 27–34.
[31] S. Zhang, Y. Zhang, J. Liu, Q. Xu, H. Xiao, X. Wang, H. Xu, J. Zhou, Thiol modified Fe_3O_4@SiO_2 as a robust, high effective, and recycling magnetic sorbent for mercury removal, Chem. Eng. J., 226 (2013) 30–38.
[32] Y. Deng, D. Qi, C. Deng, X. Zhang, D. Zhao, Superparamagnetic high-magnetization microspheres with an Fe_3O_4@SiO_2 core and perpendicularly aligned mesoporous SiO_2 shell for removal of microcystins, J. Am. Chem. Soc., 130 (2008) 28–29.
[33] X. Zhang, L. Jiang, Fabrication of novel rattle-type magnetic mesoporous carbon microspheres for removal of microcystins, J. Mater. Chem., 21 (2011) 10653.

[34] T. Liang, F. Wang, L. Liang, M. Liu, J. Sun, Magnetically separable nitrogen-doped mesoporous carbon with high adsorption capacity, J. Mater. Sci., 51 (2016) 3868–3879.
[35] J. Kim, J.E. Lee, J. Lee, J.H. Yu, B.C. Kim, K. An, Y. Hwang, C.-H. Shin, J.-G. Park, J. Kim, T. Hyeon, Magnetic fluorescent delivery vehicle using uniform mesoporous silica spheres embedded with monodisperse magnetic and semiconductor nanocrystals, J. Am. Chem. Soc., 128 (2006) 688–689.
[36] Y. Wang, J. Ren, X. Liu, Y. Wang, Y. Guo, Y. Guo, G. Lu, Facile synthesis of ordered magnetic mesoporous gamma-Fe_2O_3/SiO_2 nanocomposites with diverse mesostructures, J. Colloid Interface Sci., 326 (2008) 158–165.
[37] B.C. Kim, J. Lee, W. Um, J. Kim, J. Joo, J.H. Lee, J.H. Kwak, J.H. Kim, C. Lee, H. Lee, R.S. Addleman, T. Hyeon, M.B. Gu, J. Kim, Magnetic mesoporous materials for removal of environmental wastes, J. Hazard. Mater., 192 (2011) 1140–1147.
[38] H. Gao, Y. Sun, J. Zhou, X. Rong, H. Duan, Mussel-inspired synthesis of polydopamine-functionalized graphene hydrogel as reusable adsorbents for water purification, ACS Appl. Mater. Interfaces, 5 (2013) 425–432.
[39] H. Lee, S.M. Dellatore, W.M. Miller, P.B. Messersmith, Mussel-inspired surface chemistry for multifunctional coatings, Science, 318 (2007) 426–430.
[40] R. Liu, S.M. Mahurin, C. Li, R.R. Unocic, J.C. Idrobo, H. Gao, S.J. Pennycook, S. Dai, Dopamine as a carbon source: the controlled synthesis of hollow carbon spheres and yolk-structured carbon nanocomposites, Angew. Chem. Int. Ed., 50 (2011) 6799–6802.
[41] H. Ejima, J.J. Richardson, K. Liang, J.P. Best, M.P. van Koeverden, G.K. Such, J. Cui, F. Caruso, One-step assembly of coordination complexes for versatile film and particle engineering, Science, 341 (2013) 154–157.
[42] D. Zhou, L. Yang, L. Yu, J. Kong, X. Yao, W. Liu, Z. Xu, X. Lu, Fe/N/C hollow nanospheres by Fe(III)-dopamine complexation-assisted one-pot doping as nonprecious-metal electrocatalysts for oxygen reduction, Nanoscale, 7 (2015) 1501–1509.
[43] G. Liu, S. Zheng, D. Yin, Z. Xu, J. Fan, F. Jiang, Adsorption of aqueous alkylphenol ethoxylate surfactants by mesoporous carbon CMK-3, J. Colloid Interface Sci., 302 (2006) 47–53.
[44] W. Wang, C. Li, J. Yao, B. Zhang, Y. Zhang, J. Liu, Rapid adsorption of neutral red from aqueous solutions by $Zn_3[Co(CN)_6]_2.nH_2O$ nanospheres, J. Mol. Liq., 184 (2013) 10–16.
[45] J.K. Gao, L.A. Hou, G.H. Zhang, P. Gu, Facile functionalized of SBA-15 via a biomimetic coating and its application in efficient removal of uranium ions from aqueous solution, J. Hazard. Mater., 286 (2015) 325–333.
[46] Y. Zheng, L. Zhang, J. Shi, Y. Liang, X. Wang, Z. Jiang, Mussel-inspired surface capping and pore filling to confer mesoporous silica with high loading and enhanced stability of enzyme, Microporous Mesoporous Mater., 152 (2012) 122–127.
[47] H. Yang, Q. Lu, F. Gao, Q. Shi, Y. Yan, F. Zhang, S. Xie, B. Tu, D. Zhao, One-step synthesis of highly ordered mesoporous silica monoliths with metal oxide nanocrystals in their channels, Adv. Funct. Mater., 15 (2005) 1377–1384.
[48] H. Niu, Y. Wang, X. Zhang, Z. Meng, Y. Cai, Easy synthesis of surface-tunable carbon-encapsulated magnetic nanoparticles: adsorbents for selective isolation and preconcentration of organic pollutants, ACS Appl. Mater. Interfaces, 4 (2012) 286–295.
[49] F. Lian, G. Cui, Z. Liu, L. Duo, G. Zhang, B. Xing, One-step synthesis of a novel N-doped microporous biochar derived from crop straws with high dye adsorption capacity, J. Environ. Manage., 176 (2016) 61–68.
[50] H. Li, N. An, G. Liu, J. Li, N. Liu, M. Jia, W. Zhang, X. Yuan, Adsorption behaviors of methyl orange dye on nitrogen-doped mesoporous carbon materials, J. Colloid Interface Sci., 466 (2016) 343–351.